

Transfer learning for materials informatics using crystal graph convolutional neural network

Joohwi Lee^{1*} and Ryoji Asahi¹

¹Toyota Central R&D Laboratories, Inc., Nagakute, Aichi 480-1192, Japan

Correspondence: Joohwi Lee (j-lee@mosk.tytlabs.co.jp)

ABSTRACT

For useful applications of machine learnings in materials informatics, one challenge is to overcome inaccuracy of predictions ascribing to insufficient data. We propose a transfer learning using a crystal graph convolutional neural network (TL-CGCNN); here TL-CGCNN is pretrained with big data such as formation energies for crystal structures, and used for predictions of target properties with relatively small data. We confirm that TL-CGCNN can improve predictions for various properties such as bulk moduli, dielectric constants, and quasiparticle band gaps, which are computationally demanding to construct big data for materials. We also quantitatively observe that the more TL-CGCNN pretrains, the more accurate the prediction for the target properties by TL-CGCNN becomes. Finally, we confirm the TL-CGCNN is superior to other regression methods in the performance for the predictions with small data and conclude that TL-CGCNN is promising along with compiling big data for materials which are easy to be accumulated and relevant to the target properties.

Keywords:

transfer learning, crystal graph convolutional neural network, prediction, regression, materials informatics, TL-CGCNN

INTRODUCTION

The usage of machine learnings (ML)¹⁻⁵ has been widely applied to materials informatics (MI) field, in particular, for new materials exploration to save time and human efforts. One important challenge for the ML-based material exploration and design is to develop a generic descriptor (representation) that can be flexibly applied to predictions of multiple target properties. Because a material property depends on a crystal structure and constituent chemical elements, the descriptors have been developed based on the structural features such as Coulomb matrix,^{6,7} smooth overlap of atomic positions (SOAP),⁸⁻¹⁰ and reciprocal 3D voxel space (R3DVS)¹¹ descriptors.

Recently, Xie and Grossman introduced a crystal graph convolutional neural network (CGCNN).^{12,13} As an input for a classification or regression model by CGCNN, only a crystal structure is necessary. The CGCNN constructs crystal graphs from crystal structures and predicts the target property by a deep neural network architecture. Owing to its simplicity and flexibility, many researchers interested in graph-based neural networks have been developed for its improvement or modification. Park and Wolverton incorporated information of the Voronoi tessellated crystal structure into CGCNN to encode three body correlations.¹⁴ Sanyal *et al.*, augmented CGCNN with a multitask learning to predict multiple material properties spontaneously.¹⁵ Chen *et al.*, developed a graph network named MatERials Graph Network (MEGNet) that is extended to treat not only a crystal structure but also a molecule with additional attributes.¹⁶

Another important challenge for the ML-based materials exploration and design is to overcome unsatisfactory accuracy of predictive models ascribing to insufficient data.¹⁷ Differently from other research fields such as computer vision¹⁸ and natural language processing¹⁹ which are using big data with more than millions of data,²⁰ many functional or practical properties in MI have not been accumulated much as they are computationally or experimentally demanding for evaluation. A transfer learning²¹ is a useful method to help improving predictions suffering from insufficient data.

The transfer learning is to bring knowledge to other predictive models with different tasks (target variables). We focus on applications of transfer learning for a target model with less number of data by loading a pretrained model constructed with enormous number of data. In MI, there have been studies of using the transfer learning. For classifications of Li superionic conductors, Cubuk *et al.*,²² constructed a large number of labeled data based on crystal structure-based descriptors, and then reconstructed predictive

models based on chemical element-based descriptors by a support vector machine. Yamada *et al.*,²³ developed a pretrained model library called XenonPy.MDL²⁴ with big data for a multilayer neural network based on fingerprint descriptors,²⁵ and showed improved prediction of properties of organic or inorganic materials by the transfer learning using the neural network. Jha *et al.*,²⁶ showed an improved predictions for formation energies of smaller theoretical or experimental database by the transfer learning with a multilayer deep neural network named ElemNet,²⁷ which uses elemental composition descriptors, and pretrained models for a formation energy with larger theoretical database.^{28,29}

Indeed, in computer vision field,^{21,30-33} the transfer learning have been more widely used as deep convolutional neural network becomes the mainstream. The convolutional layers work as feature maps that can detect basic features such as vertical and horizontal lines, which are basic elements for recognizing objects. On the basis of the inspirations, CGCNN, because of its neural network architecture, may have potential for effective transfer learning in MI.

In this paper, we investigate the transfer learning using CGCNN (hereinafter called TL-CGCNN). We quantitatively confirm that the predictions for basic materials properties such as a Kohn-Sham band gap (E_g) and a formation energy (ΔE_f) can be improved by TL-CGCNN. To confirm a flexible application of the transfer learning, we also investigate whether TL-CGCNN can be useful for improving predictions for properties such as a bulk modulus (K_{VRH}),³⁴ a dielectric constant (ϵ_r),³⁵ and a quasiparticle band gap (GW- E_g),³⁶ which usually suffer from small number of data and heavy computational costs. In addition, we discuss additional issues relevant to TL-CGCNN and its prospects.

RESULTS AND DISCUSSION

CGCNN

First, we reviews background knowledge about CGCNN constructed by Xie and Grossman.^{12,13} Figure 1 shows an overview of CGCNN. The CGCNN consists of a construction of graphs based on crystal structures and a deep neural network architecture including embedding, convolutional, pooling, and fully-connected (FC) layers.

A crystal structure is transformed to a multigraph G . In the multigraph G , nodes and edges indicate atoms and chemical bonds between the atoms, respectively. The multigraph G consists of set of atoms in the crystal structure, undirected edges, atom features, and bond features. A bond feature vector ($\mathbf{u}_{(i,j)k}$) denotes the k -th bond between atoms i and j . An atom feature vector (\mathbf{v}_i) contains the properties of i -th atom. The information of atoms and bonds in the multigraph G is prepared as discrete representations consist of binary digits for describing constituent elements and bonds such as group and periodic number of atom, and atom distance. The discrete representations are transformed to continuous representations in the embedding layer. Then, the continuous representations are inserted to the convolutional layer.

In the $(t+1)$ -th convolutional layer,

$$\mathbf{v}_i^{(t+1)} = g \left[\left(\sum_{j,k} \mathbf{v}_j^{(t)} \oplus \mathbf{u}_{(i,j)k} \right) \mathbf{W}_c^{(t)} + \mathbf{v}_i^{(t)} \mathbf{W}_s^{(t)} + \mathbf{b}^{(t)} \right] \quad (1)$$

where \oplus denotes the concatenation of atom and bond feature vectors of the neighboring atoms of i th atom. $\mathbf{W}_c^{(t)}$, $\mathbf{W}_s^{(t)}$, and $\mathbf{b}^{(t)}$ indicate optimized parameters in the neural network, namely, convolution weight matrix, self weight matrix, and bias of the t -th layer, respectively. $g(\cdot)$ denote a non-linear activation function between layers such as a softplus function.³⁷

However, because the weight matrix is shared by all neighbors in this convolution formulation, different interaction of neighbors is not distinguished. Therefore, a standard edge-gating technique³⁸ can be applied for a new type of convolutional formulation as follows. A neighbor feature vector $\mathbf{z}_{(i,j)k}$ is used as,

$$\mathbf{z}_{(i,j)k}^{(t)} = \mathbf{v}_i^{(t)} \oplus \mathbf{v}_j^{(t)} \oplus \mathbf{u}_{(i,j)k}, \quad (2)$$

and then,

$$\mathbf{v}_i^{(t+1)} = \mathbf{v}_i^{(t)} + \sum_{j,k} \sigma(\mathbf{z}_{(i,j)k}^{(t)} \mathbf{W}_c^{(t)} + \mathbf{b}_c^{(t)}) \circ g(\mathbf{z}_{(i,j)k}^{(t)} \mathbf{W}_s^{(t)} + \mathbf{b}_s^{(t)}) \quad (3)$$

where \circ denotes element-wise multiplication (Hadamard product) and σ denotes a sigmoid function. Xie and Grossman¹² reported that the latter convolution formalism (equation 3) showed better predictions than the former formalism (equation 1).

The atom feature vectors after the convolutional layers are inserted into the pooling layer. Here, an average pooling³⁹ is used. After the pooling layer, a crystal feature vector (\mathbf{v}_g) can be obtained by,

$$\mathbf{v}_g = \frac{1}{N} \sum_i \mathbf{v}_i \quad (4)$$

where N is the number of atoms in the crystal graph.

Finally, \mathbf{v}_g is used as input to a network of FC layers with non-linearities which learn to predict a target property value, y , for the crystal. Predicted values can be obtained as follows,

$$\hat{y} = f(\mathbf{v}_g \mathbf{W}_g + \mathbf{b}_g) \quad (5)$$

where \mathbf{W}_g , \mathbf{b}_g , and $f(\cdot)$ are weight matrix, bias, and non-linear function of FC layers, respectively.

The parameters such as \mathbf{W} and \mathbf{b} are optimized to minimize the loss function, which is defined as mean absolute difference of predicted and target values for regressions, by a backpropagation procedure. As an optimizer, stochastic gradient descent is employed.⁴⁰

TL-CGCNN

Figure 2 shows a comparison of the concept of a conventional machine learning and a transfer learning based on a convolutional neural network. In the case of using a conventional machine learning, when we have different target variables, we prepare each predictive model separately. However, when we construct a "pretrained" (source) predictive model using a big data based on the convolutional neural networks in advance, enormous number of parameters (weight and bias) in the convolutional layer can save the features of the big data. The parameters in the convolutional layer can be transferred to the target predictive model, which have usually smaller number of training data, as "knowledge".

There are two common ways of the transfer learning to treat the loaded parameters for the convolutional neural networks. The first method is a "fine tuning". The parameters of the whole layers of the pretrained model are initially loaded. Then, all of the parameters are optimized by the backpropagation. This method is expected to have better optimization than the case of starting the optimization with randomly generated initial parameters. It is recommended to select adequate learning rate not to lose the information of the pretrained model. The second method is a "layer freezing". This method fixes the parameters of the earlier layers without additional optimizations by the backpropagation. The optimization of parameters is only performed for the latter layers to save the information from the pretrained model. In this study, we mainly used the fine tuning for TL-CGCNN.

In addition, to match the scales of target properties between pretrained and target models in this study, tanh-normalization⁴¹ was used for the predictive models as follows,

$$y' = \frac{1}{2} \left\{ \tanh\left(\frac{0.01(y-\mu)}{s}\right) + 1 \right\} \quad (6)$$

where \tanh , μ and s are hypertangent function, mean and standard deviation of target variables, y , respectively. After the predictive model is optimized, it was denormalized when the prediction error is summarized.

TL-CGCNN based on CGCNN

Before describing the results of predictions, we note that the names of pretrained and target models are written based on the number of training data and target property in this study. For example, 500-NM- E_g indicates that the target property of the predictive model is E_g , the number of training data is 500 (both numbers of validation and test data are 125), and only nonmetallic (NM) data is included in the data. Large numbers, namely, 10000, 54000, and 113000 are written as 10k, 54k, and 113k. When the number of training data is greater than 10k, the number of test data is fixed to be 2500, whereas when the number training data is less than 10k, the number of test data is set to its 25%.

Table 1 summarizes material-property dataset that used in this study. A mean absolute difference of the data indicates a baseline for a predictive model.

Figure 3 shows the dependence of prediction error of test data by CGCNN for E_g and ΔE_f on number of training data. The prediction errors decrease with increasing number of training data. When the numbers of training data reach 54k and 113k, the prediction errors for E_g and ΔE_f become 0.358 eV and 0.046 eV/atom, respectively. The prediction error of ΔE_f is comparable to the accuracy of the density functional theory (DFT) method with respect to the experiments.²⁹ We expect that the prediction error can further decrease when collecting more training data because the decreasing tendency is not saturated yet. For ΔE_f , predictive models with only NM materials data were separately constructed. When the same number of training data is used, the prediction error with only NM materials data is smaller than that with metallic and NM material data together.

However, as mentioned in Introduction, we usually suffer from unsatisfactory accuracy of predictive models ascribing to small number of data. Therefore, when we apply a TL-CGCNN to E_g and ΔE_f , we intentionally prepared target models with small number of data. The results are shown in Fig. 4, and some of

numerical values are also summarized in Supplementary Table 2. The pretrained models with large number of data for prediction targets of counterpart properties were used.

When the number of training data is 500, the prediction error for E_g by the CGCNN is 0.978 eV. By using TL-CGCNN with the 10k- ΔE_f , 54k- ΔE_f , and 113k- ΔE_f pretrained models, the prediction error decreases to 0.866, 0.826, and 0.815 eV, respectively. When the same number of training data is used, the prediction error for ΔE_f by the CGCNN is 0.239 eV/atom. When we use TL-CGCNNs with 10k-NM- E_g and 54k-NM- E_g pretrained models, the prediction error decreases to 0.236, and 0.222 eV/atom, respectively. In the both cases, the more training data we use for the pretrained models, the more the prediction powers are improved.

We also investigated the influence of data type for the transfer learning. By using only NM data, the predictive models for ΔE_f were constructed (NM- ΔE_f). When the target model is 500-NM- ΔE_f , the prediction error by TL-CGCNN with the 54k-NM- E_g pretrained model is 0.149 eV/atom, which is smaller than the case (0.184 eV/atom) that without TL-CGCNN. In addition, when the target model is 500-NM- E_g , the prediction error by TL-CGCNN with the 54k-NM- ΔE_f pretrained model is 0.819 eV smaller than that (0.826 eV) with the 54k- ΔE_f pretrained model, which used the same number of training data. This implies that when the types of participating materials in the target and pretrained models are similar to each other, TL-CGCNN for CGCNN tends to be better.

Then, we tested the dependence of TL-CGCNN on the number of data of target models. With fixing the 113k- ΔE_f pretrained model, when the target models are 500- E_g , 1000- E_g , 5000- E_g , and 10k- E_g , the prediction errors decrease from 0.866, 0.752, 0.553 to 0.490 eV, respectively. The percentage improvements of prediction error with respect to the case without transfer learning become 16.7, 12.0, 9.0 and 3.2%, which tends to decrease. With fixing the 54k-NM- E_g pretrained model, when the target models are 500- ΔE_f , and 10k- ΔE_f , the prediction errors are 0.222 and 0.089 eV/atom (7.2 and 4.6% improved with respect to predictions without TL-CGCNN), respectively. This was also tested for the prediction of ΔE_f for NM data. With fixing 54k-NM- E_g pretrained model, when the target models are 500-NM- ΔE_f , and 10k-NM- ΔE_f , the prediction errors are 0.149 and 0.065 eV/atom (19.2 and 2.8% improved with respect to predictions without TL-CGCNN), respectively. This implies that using TL-CGCNN is more efficient when we have less data.

Figure 5 shows a scatter plot between two properties of E_g and ΔE_f of 118286 materials. The scatter plot shows that there is not a strong correlation between the E_g and ΔE_f . The linear correlation coefficients (r_p) between the two properties for the total data and NM data are only -0.49 and -0.33 , respectively. For 59923 NM materials, the mean absolute error (MAE) of E_g and ΔE_f by an ordinary linear regression using ΔE_f and E_g are 1.17 eV and 0.72 eV/atom, respectively. These prediction errors are significantly larger than those by TL-CGCNN performed with only 500 training data. Despite a weak correlation, we confirmed that TL-CGCNN for E_g and ΔE_f with pretrained models based on the counterpart properties improved the predictions. This implies that atom and bond features from crystal graphs captured in the convolutional layers in the pretrained model with big data are flexibly adapted to predict various material properties.

TL-CGCNN for computationally demanding properties

We also tested TL-CGCNNs for predictive models for other properties, namely, K_{VRH} , ϵ_r , and GW- E_g . They are more computationally expensive, so that there are not so much data as E_g and ΔE_f . Note that the K_{VRH} and ϵ_r values in a \log_{10} scale were used considering their broad distributions, and the unit of the K_{VRH} value inside the \log_{10} is GPa.

Figure 6 shows prediction errors of three properties without and with TL-CGCNN. For the prediction for 500- K_{VRH} , the prediction error without TL-CGCNN is 0.123. When the 113k- ΔE_f pretrained model is used, the prediction error decreases to 0.112 (by 8.7%). For the prediction for 500-NM- ϵ_r , the prediction error without TL-CGCNN is 0.181. It also decreases to 0.169 (by 7.1%) and 0.163 (by 10.0%) when the 113k- ΔE_f and 54k-NM- E_g pretrained models are employed, respectively. Despite more training data of the 113k- ΔE_f pretrained model, the smaller prediction error of prediction based on the 54k-NM- E_g pretrained model is obtained. This may ascribe to the correlation (-0.48) between E_g and ϵ_r (in \log_{10} scale) much stronger than that (0.07) between ΔE_f and ϵ_r (in \log_{10} scale), for 4182 NM materials that have ϵ_r data. For the prediction for 180-NM-GW- E_g , the prediction error without TL-CGCNN is 0.783 eV. The smallest prediction error by TL-CGCNN among various pretrained models is achieved by the 113k- ΔE_f pretrained model, whose value decreases to 0.591 eV by 24.5%. Therefore, these results suggest that using TL-CGCNN is also useful for such practical properties.

When more data are used for prediction for K_{VRH} and ε_r , (8194 and 2788 training data for K_{VRH} and ε_r , respectively) we obtain decreased prediction error by TL-CGCNN. However, the improvement by transfer learning tends to decrease compared to the case that the target model have less data. The percentage improvements by the transfer learning for K_{VRH} and ε_r are only 1.7 and 3.7%, respectively. As the case of TL-CGCNN for E_g and ΔE_f shows, this implies that TL-CGCNN may be more useful for the predictions with small number of data.

Additional issues

We also tested predictions of 500-NM- E_g , 500- ΔE_f , 500-NM- ΔE_f , 500- K_{VRH} , and 500-NM- ε_r by partial least squares (PLS),⁴² least absolute shrinkage and selection operator (LASSO),⁴³ support vector regression (SVR),⁴⁴ and random forests (RF).⁴⁵ These widely-used regression methods were supervised using a generalized set of chemical composition based descriptors.² The results are shown in Figures 4 and 6. The numerical values are summarized in Supplementary Table S2.

The RF showed the best performance among the four regression methods. The CGCNN showed better performance on predictions of 500- ΔE_f , 500-NM- ΔE_f , and 500- K_{VRH} , but poorer performance on the predictions for 500-NM- E_g and 500-NM- ε_r than the RF. However, the TL-CGCNN could achieve the smallest prediction errors for the five predictions. The predictions with other widely-used regression methods like the RF can be improved with more specialized descriptors that have strong correlations with the target properties; however, finding additional useful descriptor for each target property is not easy. Therefore, we emphasize that the TL-CGCNN is a powerful and flexible prediction tool with merits; this tool is easy to construct pretrained models with big data, and this tool can systematically capture both features of chemical elements and crystal structures.

Deep neural networks like CGCNN have many hyperparameters. For a good transfer learning, we need to carefully select hyperparameters based on the following considerations; transferred information is to be conserved and flexibly used for the target predictive model, and overfitting is to be reduced. On the basis of the considerations, we optimized a learning rate and a length of vector of FC layer for a case study. The results are described in Supplementary chapter S1.

Until now in this study, the fine tuning has been used as the TL-CGCNN method. We also tested the layer freezing method. We only optimized the parameters of the last FC layer freezing those of the other earlier layers. As a result, for the investigated prediction targets, fine tuning showed much better predictions. The detailed results are described in Supplementary chapter S2. In some previous studies using deep convolutional neural networks with a lot of multiple layers,^{21,31} the concept of fine tuning and layer freezing are suggested to be mixed, namely, only early convolutional layers are frozen and the other layers including convolutional layers are all optimized.

In this study, TL-CGCNNs were applied for the predictive models of the various material properties, which suffer from inaccuracy ascribing to small number of data. We quantitatively confirm that the predictions can be improved by using TL-CGCNN with the pretrained model constructed with big data. Because we usually suffer from insufficient data in many MI issues, we expect that the usage of a combination of general descriptors such as CGCNN and transfer learning can be more widely employed.

METHODOLOGY

Data and evaluation of predictive model

Crystal structures, and their corresponding E_g and ΔE_f (defined with respect to the most stable state of each elemental standard state) have been compiled from a first-principles calculations database, Materials Project database (MPD).⁴⁶ They were calculated based on the exchange-correlation function of Generalized Gradient Approximation (GGA) parameterized by Perdew-Burke-Ernzerhof (PBE) form⁴⁷ in the Vienna *Ab-initio* Simulation Package (VASP).^{48,49} The on-site Coulomb interaction were treated by GGA+U in case the transition metals are included in materials.⁵⁰ We used 118286 computed data (assessed on November 11th, 2019) that is available in MPD to construct crystal graphs without a program error within a cutoff radius of 8 Å. For these data, He, Ar, and Ne were not included. Among them, 59923 data were used as NM materials under the condition, computed $E_g > 0.1$ eV. The CGCNN was applied to predict ΔE_f value with input of only crystal structures for all materials. For these NM materials, CGCNN was applied to predict E_g as well as ΔE_f value.

In this study, the ratio of training, validation, and test data was set to 4:1:1 for data selections of the CGCNN. When the number of training data is greater than 10k, the number of validation and test data were

fixed to be 2500. Weights and biases were optimized to minimize the loss function by using training data. Validation data were used to find the best epoch to stop the backpropagation with the minimum loss function, which indicates the threshold point of overfitting. Test data, which do not participate in the modeling, were used to evaluate the prediction error. In this study, a MAE of test data is used to evaluate the prediction error. The prediction errors were evaluated by averaging over several trials with different datasets. When the numbers of training data are 500, greater than 500 and less than or equal to 10k, and greater than 10k, the numbers of trials were set to 10, 5, and 2, respectively. We used random selections of training/validation/test data based on random seeds. Therefore, the same type of data could be used for comparisons of various predictive models when the same number of data are used although training/validation/test data vary among different trials. The maximum iteration of epochs was mainly set to 500 with checking that the minimum MAE of validation data is already obtained at an epoch less than 500. When this is not satisfactory, we increased the maximum iteration of epoch to until finding the minimum MAE of validation data.

The TL-CGCNNs were applied to predict E_g or ΔE_f with less data using the pretrained CGCNN models that were constructed to predict E_g or ΔE_f with 10k, 54k, and 113k (only available for ΔE_f) training data. For the target models, the ratio of the number of training, validation, and test sets were also set to 4:1:1.

To investigate the effect of TL-CGCNN on more practical cases that suffer from insufficient data, we used the target properties of K_{VRH} , ε_r , and $\text{GW-}E_g$. The K_{VRH} ³⁴ and ε_r ³⁵ values were obtained from the MPD. For the K_{VRH} , we prepared 12990 data whose values are ranged from 2 GPa (Cs metal) to 436 GPa (diamonds), and also obtained by Voigt-Reuss-Hill approximation.⁵¹ For the ε_r , we prepared 4182 NM data (with a condition of $E_g > 0.1$ eV). The ε_r value is prepared with an assumption to be a single scalar polycrystalline value converted from a dielectric tensor.³⁵ The $\text{GW-}E_g$ values were loaded from a previous study.³⁶ For $\text{GW-}E_g$ values, the G_0W_0 calculations⁵² with Heyd-Scuseria-Ernzerhof hybrid functional ($\text{G}_0\text{W}_0@\text{HSE06}$)⁵³ were used for 270 binary and ternary materials (inorganic compounds) with optimized crystal structures by PBE-sol functional.⁵⁴

Supplementary Table S1 shows main hyperparameters which were used for the CGCNN models in this study. The defaults of other hyperparameters can be referred to the original code.¹³ Among various hyperparameters, the length of feature vector of FC layer and initial learning rate were reduced for the target model when we use TL-CGCNNs.

We compared the prediction of TL-CGCNN with other widely-used regression methods for some prediction models. As the regression methods, PLS,⁴² LASSO,⁴³ SVR,⁴⁴ and RF⁴⁵ were employed. As descriptors for these regression methods, a generalized set of chemical composition-based descriptors (132 descriptors)² obtained by matminer⁵⁵ python library were used. The number of training+validation and test data were 625 and 125, respectively. For training and validation data, 5-fold cross validations were used to optimize the hyperparameters relevant to the minimization of overfitting for the regression methods.

ACKNOWLEDGEMENTS

J. L. and R. A. thank Xie and Grossman in Massachusetts Institute of Technology (MIT) for an open source code of CGCNN.¹³

AUTHOR CONTRIBUTIONS

R. A. designed the project. J. L. introduced the transfer learning function for CGCNN and performed the entire simulations in this study. All authors discussed the results and wrote the manuscript.

COMPETING INTERESTS

The authors declare no competing interests.

REFERENCE

1. Meredig, B. *et al.* Combinatorial screening for new materials in unconstrained composition space with machine learning. *Phys. Rev. B* **89**, 094104 (2014).
2. Ward, L., Agrawal, A., Choudhary, A. & Wolverton, C. A general-purpose machine learning framework for predicting properties of inorganic materials. *npj Comput. Mater.* **2**, 16028 (2016).
3. Ramprasad, R., Batra, R., Pilia, G., Mannodi-Kanakkithodi, A. & Kim, C. Machine learning in materials informatics: recent applications and prospects. *npj Comput. Mater.* **3**, 54 (2017).
4. Butler, K. T., Davies, D. W., Cartwright, H., Isayev, O. & Walsh, A. Machine learning for molecular and materials science. *Nature* **559**, 547 (2018).
5. Schmidt, J., Marques, M. R., Botti, S. & Marques, M. A. Recent advances and applications of machine learning in solid-state materials science. *npj Comput. Mater.* **5**, 83 (2019).
6. Rupp, M., Tkatchenko, A., Müller, K.-R. & Von Lilienfeld, O. A. Fast and accurate modeling of molecular atomization energies with machine learning. *Phys. Rev. Lett.* **108**, 058301 (2012).
7. Montavon, G. *et al.* Machine learning of molecular electronic properties in chemical compound space. *New J. Phys.* **15**, 095003 (2013).
8. Bartók, A. P., Kondor, R. & Csányi, G. On representing chemical environments. *Phys. Rev. B* **87**, 184115 (2013).
9. De, S., Bartók, A. P., Csányi, G. & Ceriotti, M. Comparing molecules and solids across structural and alchemical space. *Phys. Chem. Chem. Phys.* **18**, 13754–13769 (2016).
10. Jinnouchi, R. & Asahi, R. Predicting catalytic activity of nanoparticles by a DFT-aided machine-learning algorithm. *J. Phys. Chem. Lett.* **8**, 4279–4283 (2017).
11. Kajita, S., Ohba, N., Jinnouchi, R. & Asahi, R. A universal 3D voxel descriptor for solid-state material informatics with deep convolutional neural networks. *Sci. Rep.* **7**, 16991 (2017).
12. Xie, T. & Grossman, J. C. Crystal graph convolutional neural networks for an accurate and interpretable prediction of material properties. *Phys. Rev. Lett.* **120**, 145301 (2018).

13. CGCNN (compatible with pytorch ver. 0.3.1), <https://github.com/txie-93/cgcnn> (Last accessed Feb. 20, 2019).
14. Park, C. W. & Wolverton, C. Developing an improved Crystal Graph Convolutional Neural Network framework for accelerated materials discovery. Preprint at <https://arxiv.org/abs/1906.05267> (2019).
15. Sanyal, S. *et al.* MT-CGCNN: Integrating Crystal Graph Convolutional Neural Network with Multitask Learning for Material Property Prediction. Preprint at <https://arxiv.org/abs/1811.05660> (2018).
16. Chen, C., Ye, W., Zuo, Y., Zheng, C. & Ong, S. P. Graph networks as a universal machine learning framework for molecules and crystals. *Chem. Mater.* **31**, 3564–3572 (2019).
17. Zhang, Y. & Ling, C. A strategy to apply machine learning to small datasets in materials science. *npj Comput. Mater.* **4**, 25 (2018).
18. LeCun, Y., Bengio, Y. & Hinton, G. Deep learning. *Nature* **521**, 436 (2015).
19. Young, T., Hazarika, D., Poria, S. & Cambria, E. Recent trends in deep learning based natural language processing. *IEEE Comput. Intell. M.* **13**, 55–75 (2018).
20. Deng, J. *et al.* Imagenet: A large-scale hierarchical image database. in *2009 IEEE conference on computer vision and pattern recognition* 248–255 (IEEE, 2009).
21. Yosinski, J., Clune, J., Bengio, Y. & Lipson, H. How transferable are features in deep neural networks? in *Advances in Neural Information Processing Systems 27*. (eds Ghahramani, Z. *et al.*) 3320–3328 (Curran Associates, Inc., 2014).
22. Cubuk, E. D., Sendek, A. D. & Reed, E. J. Screening billions of candidates for solid lithium-ion conductors: A transfer learning approach for small data. *J. Chem. Phys.* **150**, 214701 (2019).
23. Yamada, H. *et al.* Predicting Materials Properties with Little Data Using Shotgun Transfer Learning. *ACS Cent. Sci.* **5**, 1717–1730 (2019).
24. XenonPy, <https://github.com/yoshida-lab/XenonPy>, (Last accessed Feb. 18, 2020).

25. *RDKit: open-Source cheminformatics software*. <http://www.rdkit.org>, (Last accessed Feb. 18, 2020).
26. Jha, D. *et al.* Enhancing materials property prediction by leveraging computational and experimental data using deep transfer learning. *Nat. Comm.* **10**, 5316 (2019).
27. Jha, D. *et al.* Elemnet: Deep learning the chemistry of materials from only elemental composition. *Sci. Rep.* **8**, 17593 (2018).
28. Saal, J. E., Kirklin, S., Aykol, M., Meredig, B. & Wolverton, C. Materials design and discovery with high-throughput density functional theory: the open quantum materials database (OQMD). *JOM* **65**, 1501–1509 (2013).
29. Kirklin, S. *et al.* The Open Quantum Materials Database (OQMD): assessing the accuracy of DFT formation energies. *npj Comput. Mater.* **1**, 15010 (2015).
30. Hoffman, J. *et al.* LSDA: Large scale detection through adaptation. in *Advances in Neural Information Processing Systems 27*. (eds Ghahramani, Z. *et al.*) 3536–3544 (Curran Associates, Inc., 2014).
31. Soekhoe, D., Van Der Putten, P. & Plaat, A. On the impact of data set size in transfer learning using deep neural networks. in *15th International Symposium on Intelligent Data Analysis*. (eds Boström, H., Knobbe, A., Soares, C., & Papapetrou, P.) 50–60 (Springer, 2016).
32. Gopalakrishnan, K., Khaitan, S. K., Choudhary, A. & Agrawal, A. Deep Convolutional Neural Networks with transfer learning for computer vision-based data-driven pavement distress detection. *Constr. Build. Mater.* **157**, 322–330 (2017).
33. Kensert, A., Harrison, P. J. & Spjuth, O. Transfer learning with deep convolutional neural networks for classifying cellular morphological changes. *SLAS Discov.* **24**, 466–475 (2019).
34. De Jong, M. *et al.* Charting the complete elastic properties of inorganic crystalline compounds. *Sci. Data* **2**, 150009 (2015).

35. Petousis, I. *et al.* High-throughput screening of inorganic compounds for the discovery of novel dielectric and optical materials. *Sci. Data* **4**, 160134 (2017).
36. Lee, J., Seko, A., Shitara, K., Nakayama, K. & Tanaka, I. Prediction model of band gap for inorganic compounds by combination of density functional theory calculations and machine learning techniques. *Phys. Rev. B* **93**, 115104 (2016).
37. Dugas, C., Bengio, Y., Bélisle, F., Nadeau, C. & Garcia, R. Incorporating second-order functional knowledge for better option pricing. in *Advances in Neural Information Processing Systems 13*. (eds Leen, T. K., Dietterich, T. G., & Tresp, V.) 472–478 (MIT Press, 2001).
38. Marcheggiani, D. & Titov, I. Encoding Sentences with Graph Convolutional Networks for Semantic Role Labeling. in *Proceedings of the 2017 Conference on Empirical Methods in Natural Language Processing*. (eds Palmer, M., Hwa, R., & Riedel, S.) 1506–1515 (Association for Computational Linguistics, 2017).
39. Duvenaud, D. K. *et al.* Convolutional networks on graphs for learning molecular fingerprints. in *Advances in neural information processing systems 28*. (eds Cortes, C. *et al.*) 2224–2232 (Curran Associates, Inc., 2015).
40. Bottou, L. & Bousquet, O. The tradeoffs of large scale learning. in *Advances in neural information processing systems 20*. (eds Platt, J. C., Koller, D., Singer, Y., & Roweis, S. T.) 161–168 (Curran Associates, Inc., 2008).
41. Jain, A., Nandakumar, K. & Ross, A. Score normalization in multimodal biometric systems. *Pattern Recognit.* **38**, 2270–2285 (2005).
42. Geladi, P. & Kowalski, B. R. Partial least-squares regression: a tutorial. *Anal. Chim. Acta.* **185**, 1–17 (1986).
43. Tibshirani, R. Regression Shrinkage and Selection via the Lasso. *J. Royal Stat. Soc. B* **58**, 267–288 (1996).

44. Smola, A. & Schölkopf, B. A tutorial on support vector regression. *Stat. Comput.* **14**, 199–222 (2004).
45. Liaw, A. & Wiener, M. Classification and regression by randomForest. *R news* **2**, 18–22 (2002).
46. Jain, A. *et al.* Commentary: The Materials Project: A materials genome approach to accelerating materials innovation. *Appl. Phys. Lett. Mater.* **1**, 011002 (2013).
47. Perdew, J. P., Burke, K. & Ernzerhof, M. Generalized gradient approximation made simple. *Phys. Rev. Lett.* **77**, 3865–3868 (1996).
48. Kresse, G. & Furthmüller, J. Efficiency of ab-initio total energy calculations for metals and semiconductors using a plane-wave basis set. *Comput. Mater. Sci.* **6**, 15–50 (1996).
49. Kresse, G. & Furthmüller, J. Efficient iterative schemes for *ab initio* total-energy calculations using a plane-wave basis set. *Phys. Rev. B* **54**, 11169–11186 (1996).
50. Dudarev, S. L., Botton, G. A., Savrasov, S. Y., Humphreys, C. J. & Sutton, A. P. Electron-energy-loss spectra and the structural stability of nickel oxide: An LSDA+U study. *Phys. Rev. B* **57**, 1505–1509 (1998).
51. Chung, D. & Buessem, W. The Voigt - Reuss - Hill Approximation and Elastic Moduli of Polycrystalline MgO, CaF₂, β - ZnS, ZnSe, and CdTe. *J. Appl. Phys.* **38**, 2535–2540 (1967).
52. Fuchs, F., Furthmüller, J., Bechstedt, F., Shishkin, M. & Kresse, G. Quasiparticle band structure based on a generalized Kohn-Sham scheme. *Phys. Rev. B* **76**, 115109 (2007).
53. Heyd, J., Scuseria, G. E. & Ernzerhof, M. Erratum: “Hybrid functionals based on a screened Coulomb potential” [*J. Chem. Phys.* **118**, 8207 (2003)]. *J. Chem. Phys.* **124**, 219906 (2006).
54. Perdew, J. *et al.* Restoring the Density-Gradient Expansion for Exchange in Solids and Surfaces. *Phys. Rev. Lett.* **100**, 136406 (2008).
55. Ward, L. *et al.* Matminer: An open source toolkit for materials data mining. *Comput. Mater. Sci.* **152**, 60–69 (2018).

56. Scott, D. W. *Multivariate density estimation: theory, practice and visualization*. 1st edn, (Wiley, 1992).

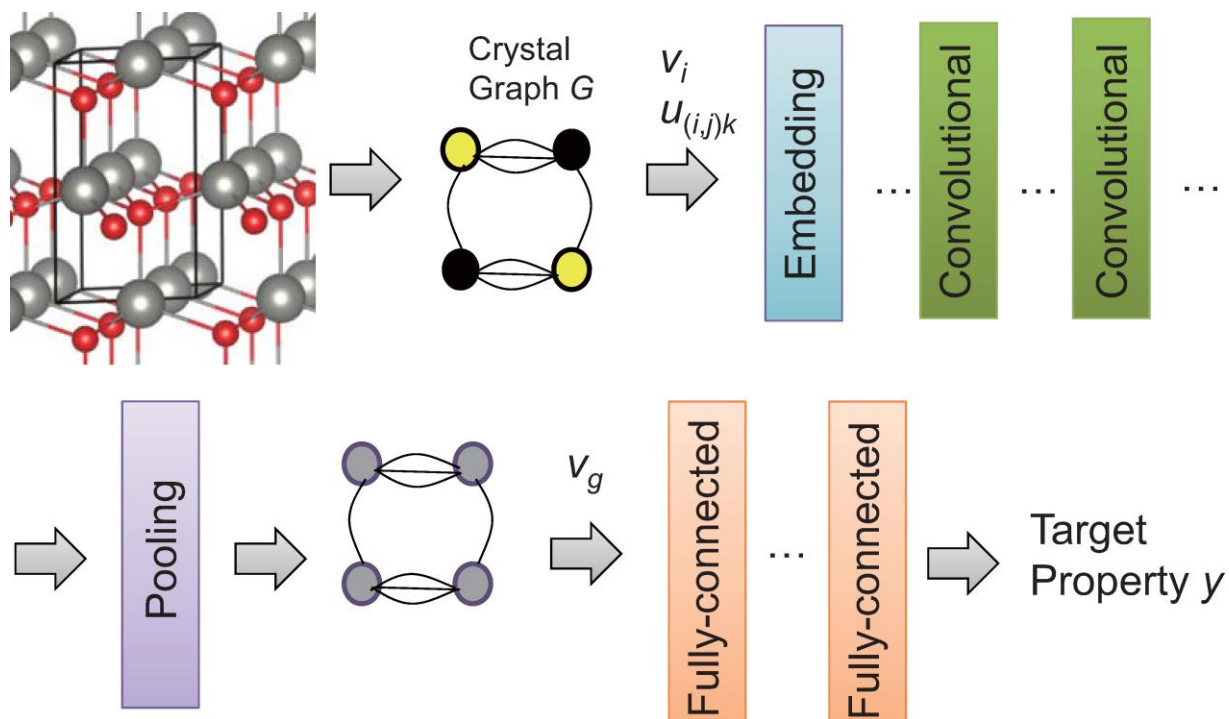


Fig. 1 Overview of CGCNN. It predicts a target property with an input of crystal structure, which is transformed into a crystal graph. The CGCNN architecture consists of embedding, convolutional, pooling, and fully-connected layers.

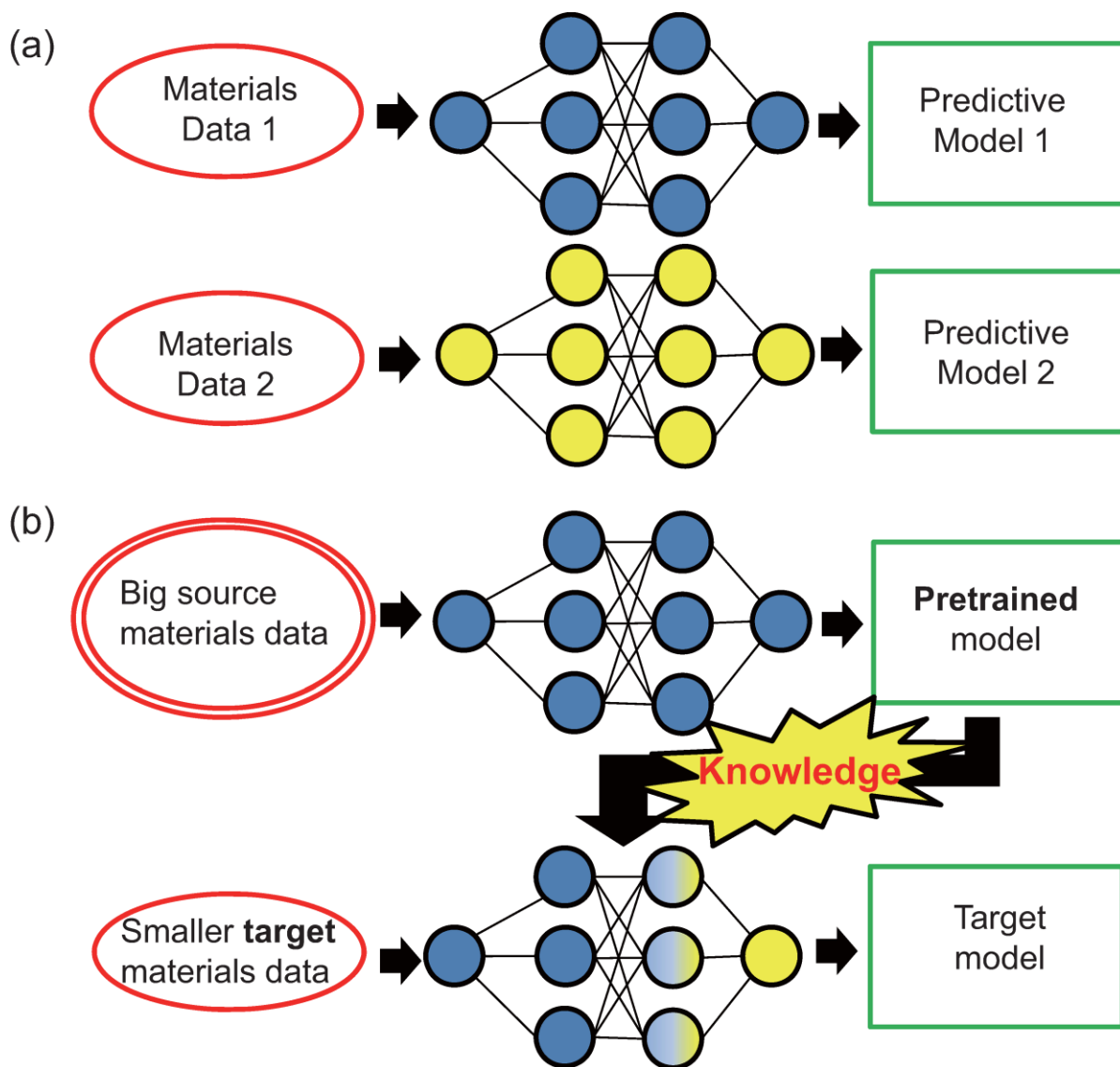


Fig. 2 Overview of transfer learning. Comparison of (a) a conventional learning and (b) its transfer learning. When we have different tasks, we prepare different prediction models separately for a conventional learning case. When we use the transfer learning, the knowledge (parameters, namely, weights and biases) accumulated in the pretrained model with a big data, can be transferred to target prediction model.

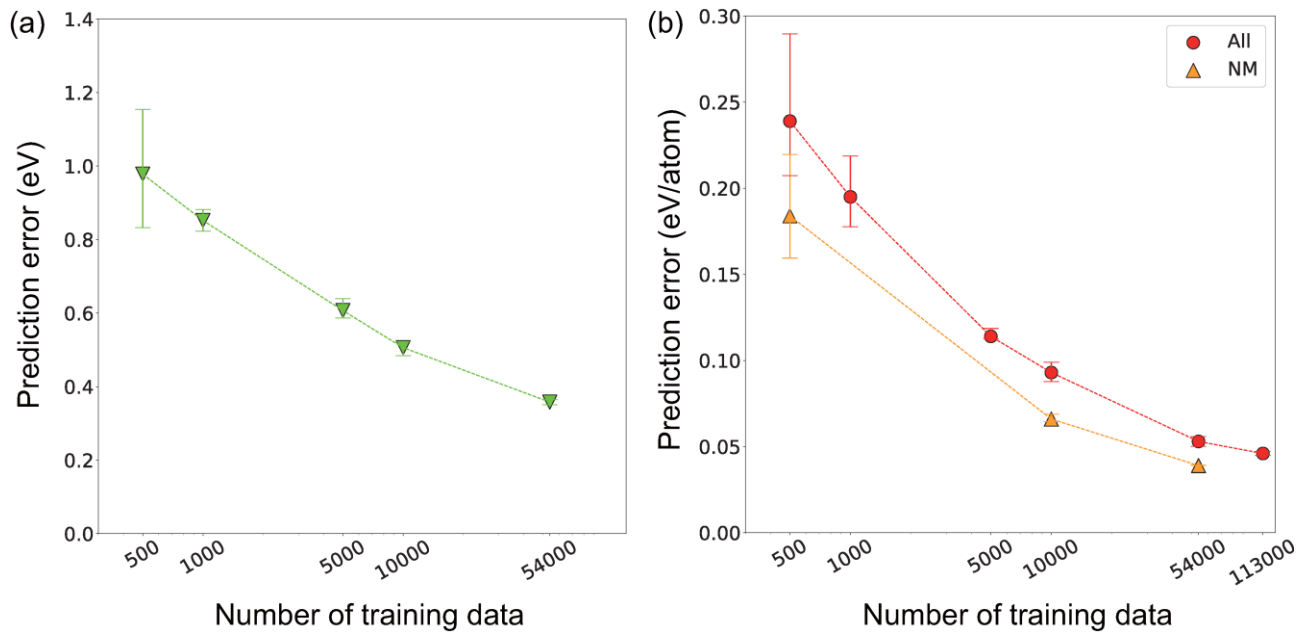


Fig. 3 Dependence of prediction error (RMSE of test data). Prediction errors for (a) E_g and (b) ΔE_f on number of training data. Horizontal axes are in \log_{10} scale. Error bars indicate the maximum and minimum values of several trials.

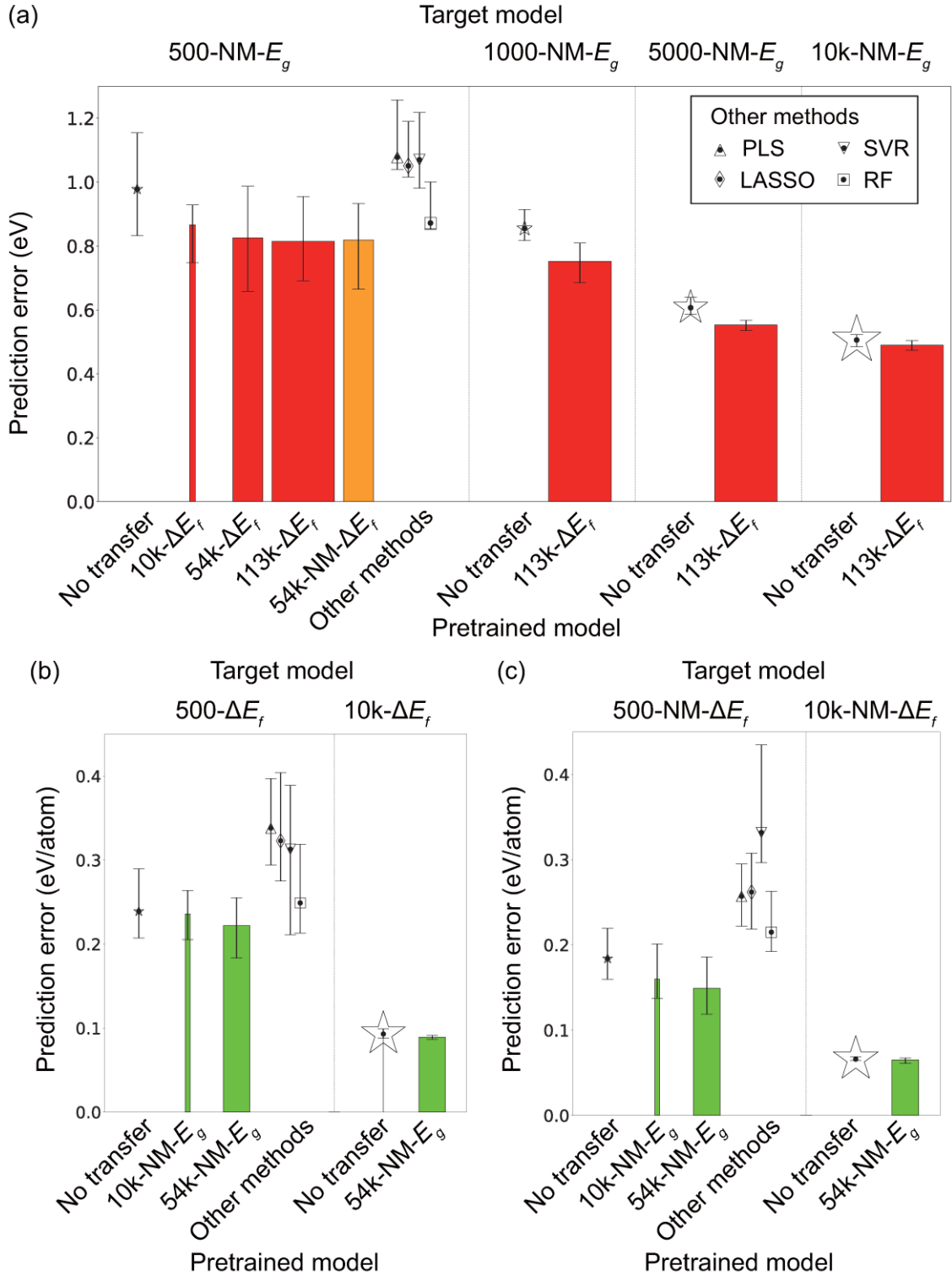


Fig. 4 Comparison of prediction error of without and with pretrained models. Prediction errors for (a) E_g , (b) ΔE_f , and (c) NM(nonmetallic)- ΔE_f . The predictions by the CGCNN and other regression methods are displayed as scatter plots. The predictions by the TL-CGCNN are displayed as bar graphs. The number of training data of target and pretrained models are displayed as relative size of scatter plot and relative width of bar graph, respectively. Error bars indicate the maximum and minimum values of several trials. The baselines, obtained as the mean absolute differences of the data distribution, for E_g , ΔE_f , and NM- ΔE_f are 1.26, 0.97, and 0.77 (in the same unit as in each subfigure), respectively.

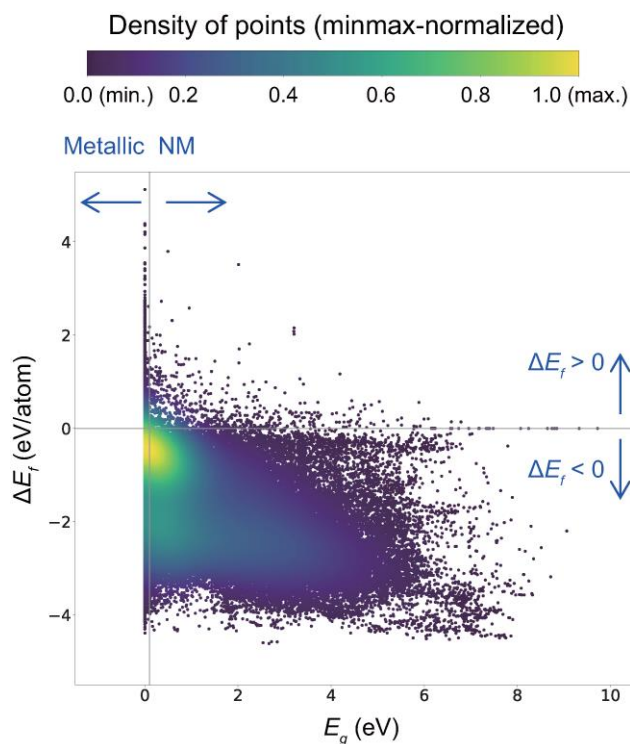


Fig. 5 Scatter plots between the quantities of ΔE_f and E_g of 118286 materials. The color scale represents the relative density of points generated by Gaussian kernel density estimation.⁵⁶ The probability density function is minmax-normalized, and the bandwidth for Gaussian is three times multiplied by Scott's factor.⁵⁶

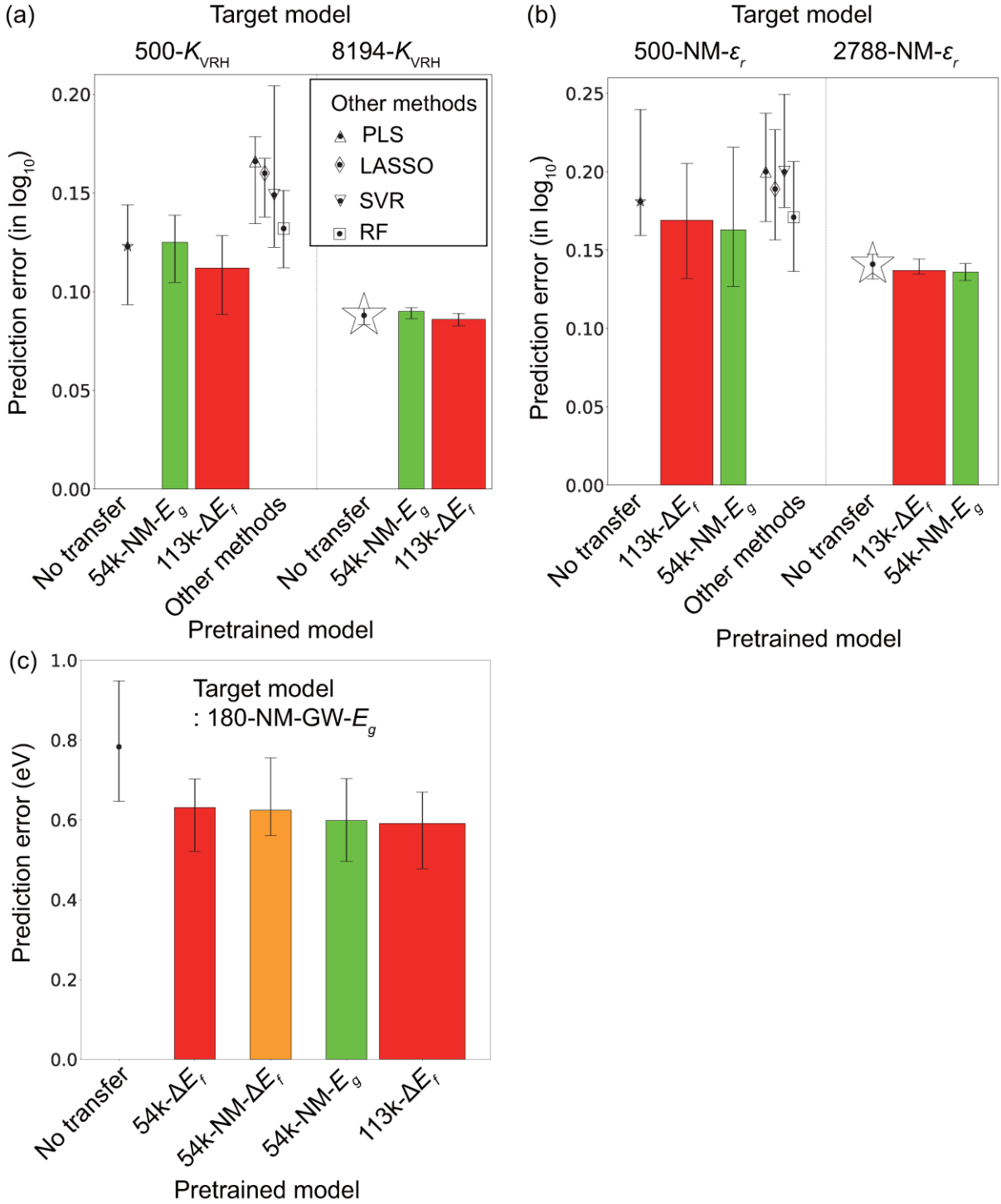


Fig. 6 Comparison of prediction error of without and with pretrained models. Prediction errors of (a) K_{VRH} , (b) ϵ_r , and (c) $\text{GW-}E_g$ without and with pretrained models. The predictions by the CGCNN and other regression methods are displayed as scatter plots. The predictions by the TL-CGCNN are displayed as bar graphs. The number of training data of target and pretrained models are displayed as relative size of scatter plot and relative width of bar graph, respectively. The unit of K_{VRH} in \log_{10} is GPa. Error bars indicate the maximum and minimum values of several trials. The baselines, obtained as the mean absolute differences of the data distribution, for K_{VRH} , ϵ_r , and $\text{GW-}E_g$ are 0.30, 0.27, and 2.49 (in the same unit as in each subfigure), respectively.

Table 1. Summary of material-property dataset used in this study.

Material Property	Number of data	Minimum value	Maximum value	Mean value	Mean absolute difference
E_g	59923	0.100 eV	9.721 eV	2.179 eV	1.256 eV
ΔE_f	118286	-4.612 eV/atom	5.124 eV/atom	-1.481 eV/atom	0.968 eV/atom
ΔE_f (NM)	59923	-4.612 eV/atom	3.797 eV/atom	-2.021 eV/atom	0.768 eV/atom
K_{VRH} ^{a,b}	12990	0.301	2.639	1.874	0.304
ϵ_r ^a	4182	0.063	2.992	1.096	0.265
GW- E_g	270	0.357 eV	14.548 eV	4.996 eV	2.486 eV

^a The values are in \log_{10} .

^b The unit in \log_{10} is GPa.

Supporting Information

S1. Optimization of hyperparameters for TL-CGCNN

Deep neural networks like CGCNN have many hyperparameters. For a strict optimization, all the hyperparameters must be optimized. However, it needs heavy computations to optimize such a large set of hyperparameters. In this study, we tried to test the influence of learning rate and length of feature vector of FC layer on the prediction error by TL-CGCNN with fixing other hyperparameters summarized in Supplementary Table S1. We use a case study of predictive model for the 500-NM- E_g by TL-CGCNN with the 113k- ΔE_f pretrained model.

A learning rate for the optimization of weight and bias is determined by an initial learning rate and a learning rate decay. At early epochs, the initial learning rate becomes the learning rate. Then, the learning rate can be decayed by a multiplicative factor at later epochs. In addition, there can be many combinations relevant to a modifying schedule for the learning rate, such as the frequency of decay and the epochs that decay occurs. In this study, we only check the initial learning rate and multiplicative factor of learning rate decay.

Figure S1a shows the prediction error for the 500-NM- E_g depending on the initial learning rate. The initial learning rate of the pretrained model is 0.01. When the initial learning rate is too large as 1, the prediction errors are larger. This may ascribe to that the optimized parameters loaded from the pretrained models may disappear. The smallest prediction error is obtained when the initial learning rate is 0.005. Therefore, for the "fine" tuning, it is recommended to use an adequately small learning rate, not to lose the transferred knowledge. However, when the learning rate is too small as 0.0001, the prediction error increases again. This means that an effective learning was not performed.

Figure S1b shows the prediction error for the 500-NM- E_g depending on the multiplicative factor of learning rate decay. The multiplicative factor of learning rate decay of the pretrained model is 0.1. The smallest prediction error is obtained when the multiplicative factor of learning rate decay is 0.0001. At the investigated range of 0.0001–10 for the multiplicative factor of learning rate decay, the differences of the prediction errors are not so large as those by change of the initial learning rate. This may ascribe to that

whether transferred knowledge is conserved or not strongly depends on the initial learning rate at early epochs for this predictive model.

Figure S1c shows the prediction error for the 500-NM- E_g depending on the length of feature vector of FC layer of the target model. In the pretrained model, the length of feature vector of FC layer is 128. The smallest prediction error is obtained when the length of feature vector of FC layer is 64. The prediction errors are similar with the values of 0.815–0.836 eV when the lengths of feature vector of FC layer are 4–256. However, we recommend not using too small or large length of feature vector of FC layer, which can result in much larger prediction errors.

Table S1. Main hyperparameters used for CGCNN and TL-CGCNN in this study.

Hyperparameters	Value
Minibatch size	256
Length of atom feature vector v_i after an embedding layer	64
Number of convolutional layers	3
Length of feature vector of FC layer	128→64 (in case of transfer learning)
Number of FC layer	1
Optimizer for loss function	Stochastic gradient descent
Initial learning rate	0.01→0.005 (in case of transfer learning)
Multiplicative factor of learning rate decay ^a	0.1
Dropout	0

^a In the CGCNN code, the learning rate decay occurs at the 100th epoch as a default.

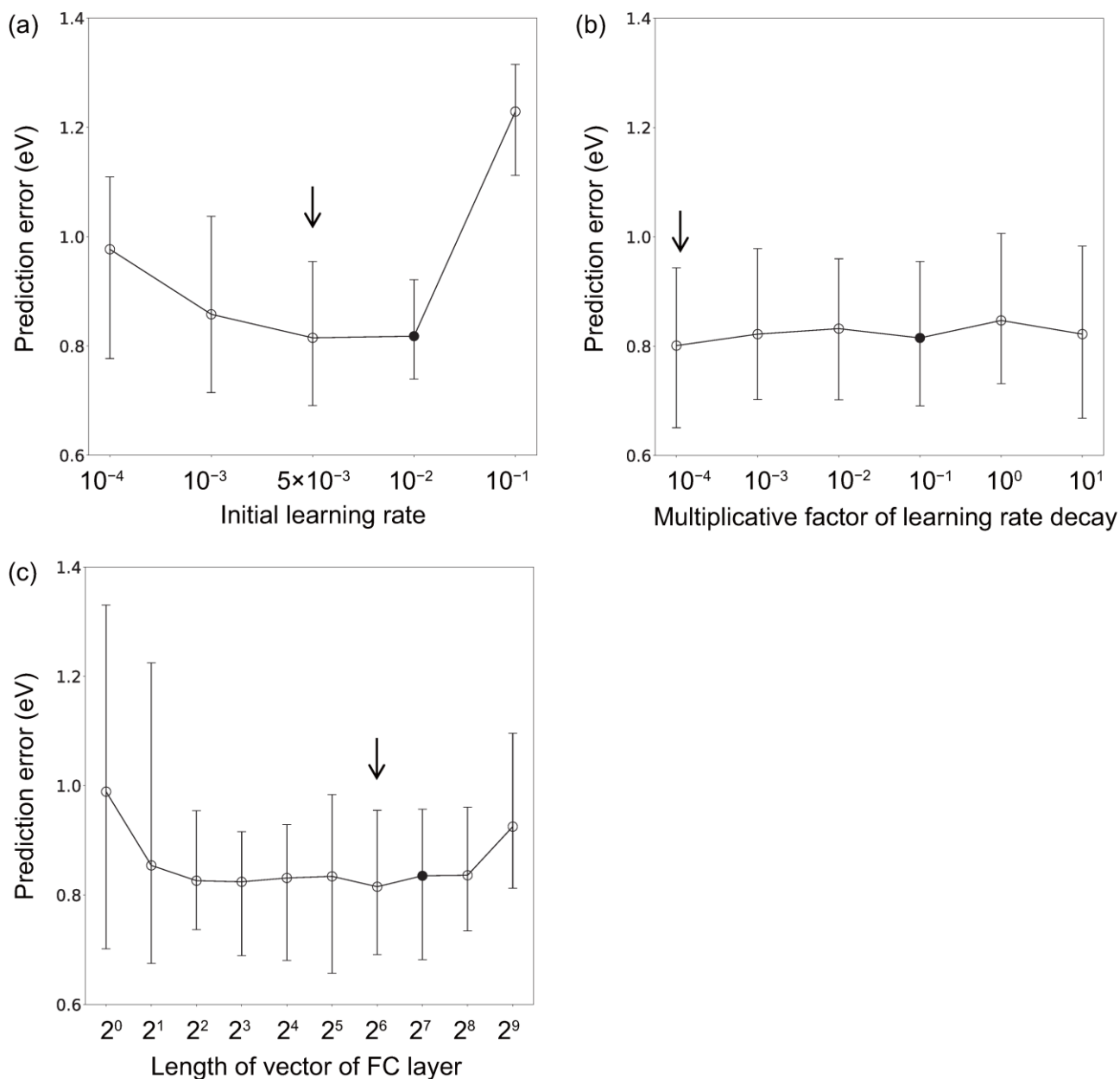


Fig. S1. Dependences of prediction error of transfer learning on hyperparameters. Prediction error for the 500-NM-*Eg* prediction model depending on (a) initial learning rates, (b) learning rate decays, and (c) lengths of vector of FC layer by transfer learning with the 113k- ΔE_f pretrained model. Closed marks indicate the hyperparameter used in the pretrained model. A vertical indicator shows the optimal hyperparameter with the smallest prediction error. Error bars indicate the maximum and minimum values of several trials.

S2. Test of layer freezing

In this study, the fine tuning has been used as the TL-CGCNN. For a comparison, the layer freezing is also investigated as the TL-CGCNN. We only optimized the weights and biases of the last FC layer with freezing those of the other earlier layers. For the prediction targets, the 500-NM- E_g , 500- ΔE_f , 500-NM- ΔE_f , 500- K_{VRH} , 500-NM- ε_r , and 180-NM-GW- E_g were used with the 113k- ΔE_f , 54k-NM- E_g , 54k-NM- E_g , 113k- ΔE_f , 54k-NM- E_g , and 113k- ΔE_f pretrained models, respectively, which showed the best performance when the fine tuning is used. The identical hyperparameters were used for two methods. Supplementary Table S2 summarizes the comparison of the prediction errors by the CGCNN, the fine tuning, the layer freezing, and other regression methods. The prediction errors of training data are also shown.

For all of six predictive models by the TL-CGCNN, the fine tuning shows much smaller prediction errors than layer freezing. In the case of the 500-NM- E_g target model, the layer freezing shows prediction error of 0.956 eV slightly smaller than that of 0.978 eV by the prediction without a TL-CGCNN. However, in the cases of the 500- ΔE_f , 500-NM- ΔE_f , 500- K_{VRH} , 500-NM- ε_r , and 180-NM-GW- E_g target models, the layer freezing shows even worse predictions than those without the transfer learning.

Although the prediction improvements are not achieved by the layer freezing, the prediction error differences between the training data and test data are much smaller than those obtained by the fine tuning. This means that the overfitting is reduced. However, relatively larger errors of training data obtained by the layer freezing indicate that the freezing of parameters of the convolutional layers in CGCNN obstructs the optimization of the predictive model to a satisfying level. In some previous studies using deep convolutional neural networks with a lot of multiple layers,^{1,2} the concept of two methods are suggested to be mixed, namely, only early convolutional layers are frozen and the other layers including convolutional layers are all optimized.

Table S2. Comparison of prediction error (as MAE) of training and test data by the CGCNN, fine tuning, layer freezing, and other regression methods. The bold model emphasizes the smallest error of test data. The value in the parentheses is standard deviation of MAE of ten trials. Note that different training/validation/test data are used for each trial.

Target model	Pretrained model	Method	Prediction error of training data	Prediction error of test data ^c	Unit
500-NM- E_g		CGCNN	0.576 (0.129)	0.978 (0.113)	eV
500-NM-E_g	113k-ΔE_f	Fine tuning by TL-CGCNN	0.511 (0.144)	0.815 (0.090)	eV
500-NM- E_g	113k- ΔE_f	Layer freezing by TL-CGCNN	0.919 (0.046)	0.956 (0.099)	eV
500-NM- E_g		PLS	0.940 (0.021)	1.051 (0.066)	eV
500-NM- E_g		LASSO	0.850 (0.021)	1.078 (0.084)	eV
500-NM- E_g		SVR	0.720 (0.033)	1.070 (0.087)	eV
500-NM- E_g		RF	0.367 (0.038)	0.872 (0.060)	eV
500- ΔE_f		CGCNN	0.092 (0.018)	0.239 (0.026)	eV/atom
500-ΔE_f	54k-NM-E_g	Fine tuning by TL-CGCNN	0.083 (0.030)	0.222 (0.024)	eV/atom
500- ΔE_f	54k-NM- E_g	Layer freezing by TL-CGCNN	0.443 (0.021)	0.482 (0.055)	eV/atom
500- ΔE_f		PLS	0.268 (0.016)	0.338 (0.038)	eV/atom
500- ΔE_f		LASSO	0.301 (0.026)	0.323 (0.044)	eV/atom
500- ΔE_f		SVR	0.224 (0.071)	0.313 (0.051)	eV/atom
500- ΔE_f		RF	0.103 (0.007)	0.249 (0.033)	eV/atom
500-NM- ΔE_f		CGCNN	0.081 (0.022)	0.184 (0.023)	eV/atom
500-NM-ΔE_f	54k-NM-E_g	Fine tuning by TL-CGCNN	0.059 (0.006)	0.149 (0.021)	eV/atom
500-NM- ΔE_f	54k-NM- E_g	Layer freezing by TL-CGCNN	0.371 (0.018)	0.424 (0.033)	eV/atom
500-NM- ΔE_f		PLS	0.211 (0.010)	0.257 (0.022)	eV/atom
500-NM- ΔE_f		LASSO	0.237 (0.025)	0.262 (0.023)	eV/atom
500-NM- ΔE_f		SVR	0.222 (0.045)	0.332 (0.042)	eV/atom
500-NM- ΔE_f		RF	0.093 (0.004)	0.215 (0.020)	eV/atom
500- K_{VRH}		CGCNN	0.067 (0.020)	0.123 (0.015)	a,b
500-K_{VRH}	113k-ΔE_f	Fine tuning by TL-CGCNN	0.075 (0.022)	0.112 (0.012)	a,b
500- K_{VRH}	113k- ΔE_f	Layer freezing by TL-CGCNN	0.149 (0.008)	0.161 (0.011)	a,b
500- K_{VRH}		PLS	0.132 (0.008)	0.166 (0.013)	a,b
500- K_{VRH}		LASSO	0.145 (0.007)	0.160 (0.009)	a,b
500- K_{VRH}		SVR	0.075 (0.039)	0.149 (0.024)	a,b
500- K_{VRH}		RF	0.059 (0.008)	0.132 (0.012)	a,b
500-NM- ϵ_r		CGCNN	0.120 (0.032)	0.181 (0.024)	a
500-NM-ϵ_r	54k-NM-E_g	Fine tuning by TL-CGCNN	0.095 (0.016)	0.163 (0.024)	a
500-NM- ϵ_r	54k-NM- E_g	Layer freezing by TL-CGCNN	0.181 (0.008)	0.193 (0.032)	a
500-NM- ϵ_r		PLS	0.165 (0.006)	0.200 (0.020)	a
500-NM- ϵ_r		LASSO	0.175 (0.005)	0.189 (0.021)	a
500-NM- ϵ_r		SVR	0.074 (0.031)	0.200 (0.024)	a
500-NM- ϵ_r		RF	0.079 (0.010)	0.171 (0.019)	a
180-NM-GW- E_g		CGCNN	0.302 (0.140)	0.783 (0.102)	eV
180-NM-GW-E_g	113k-ΔE_f	Fine tuning by TL-CGCNN	0.196 (0.082)	0.591 (0.063)	eV
180-NM-GW- E_g	113k- ΔE_f	Layer freezing by TL-CGCNN	0.525 (0.178)	0.867 (0.152)	eV

^a The values are in \log_{10} .

^b The unit in \log_{10} is GPa.

^c Note that number of test data is 25% of that of training data.

Supplementary Reference

1. Yosinski, J., Clune, J., Bengio, Y. & Lipson, H. How transferable are features in deep neural networks? in *Advances in Neural Information Processing Systems 27*. (eds Ghahramani, Z. *et al.*) 3320–3328 (Curran Associates, Inc., 2014).
2. Soekhoe, D., Van Der Putten, P. & Plaat, A. On the impact of data set size in transfer learning using deep neural networks. in *15th International Symposium on Intelligent Data Analysis*. (eds Boström, H., Knobbe, A., Soares, C., & Papapetrou, P.) 50–60 (Springer, 2016).